RSC Advances

ROYAL SOCIETY OF CHEMISTRY

www.rsc.org/advances

Enhanced power factor in flexible reduced graphene oxide/nanowires hybrid films for thermoelectrics

Jie Gao[a,b], Chengyan Liu[b], Lei Miao[b,*], Xiaoyang Wang[b], Ying Peng[b], Yu Chen[a,*]

[a] Key Laboratory for Advanced Materials, School of Chemistry and Molecular Engineering , East China University of Science and Technology, 130 Meilong Road, Shanghai 200237, China.

[b] Guangxi Key Laboratory of Information Material, Guangxi Collaborative Innovation Center of Structure and Property for New Energy and Materials, School of Material Science and Engineering, Guilin University of ElectronicTechnology, Guilin, 541004, P. R. China.

* Corresponding authors.

E-mail address: miaolei@guet.edu.cn (Lei Miao) , chentangyu@yahoo.com (Yu Chen).

Abstract

Highly-flexible thermoelectric hybrid films based on the reduced graphene oxide (RGO) and tellurium nanowires (Te NWs) layered structure are fabricated via vacuum filtration. The electrical conductivity and Seebeck coefficient of the optimized hybrid film can reach 978 S/m and 286 μV/K, respectively, pushing the power factor (PF) value up to 80 μW/(mK^2) at 40^{o}C, approximately 80 times larger than the pure Te NWs film, possibly due to the combination of high carrier concentration of RGO and high carrier mobility of Te NWs. Meanwhile, the transport characteristics of hybrid films were revealed by the measurements of electrical conductivity, Seebeck coefficient, and Hall effect. This article provides a possible access to high-performance and flexible TE films based on RGO sheets and inorganic semiconductors.

1. Introduction

With the ability to directly convert temperature gradient to voltage difference or vice versa, thermoelectric (TE) materials have shown promising potential in applications on electronic cooling devices and energy harvesting system [1-3]. The efficiency of thermoelectric materials is usually determined by a dimensionless figure of merit $ZT = (S^2\sigma T)/\kappa$, where S is the Seebeck coefficient, σ is the electrical conductivity, T is the absolute temperature, and κ is the total thermal conductivity due to both phonons and electrons, respectively. When the data for κ is not available, the material can also be evaluated by the power factor ($PF=S^2\sigma$), which quantifies the ability of a given material to generate useful power, without comment on the efficiency [4]. During the recent decade, flexible thermoelectric materials for portable/wearable electronic devices have attracted extensive attention [5-6], but the traditional inorganic bulk thermoelectric materials are still stiff and brittle, making them unsuitable for practical applications.

With the reduced dimensionality and size, inorganic materials would become flexible to some degree [7]. Nevertheless, the flexibility of nanosized inorganic materials is too poor to fabricate thermoelectric films by themselves [8]. Due to the advantage of being flexible and facile to synthesize and process, the conductive polymers and inorganic nanostructure / conductive polymer composites [9-10] have been gradually applied in flexible thermoelectric materials. For instance, a tosylate doped poly(3,4-ethylenedioxythiophene) (PEDOT) with ZT = 0.25 [11] and a poly(styrenesulfonate) (PSS) doped PEDOT with ZT = 0.42 [12] were successively reported. As to the composites consisting of inorganic semiconductors and conductive polymers, Yao et al [13] reported an enhanced PF value in polyaniline / carbon nanotube (PANI / CNT) composites and See et al. synthesized a water-processable hybrid film based on PEDOT:PSS and tellurium (Te) nanocrystal with ZT = 0.1 [14]. By rationally engineering the organic–inorganic semiconductor interfaces of polymer composites, the improvement of the S and PF in the poly (3-hexylthiophene)/Bi_2Te_3 nanowires was realized [15]. However, the PEDOT: PSS dispersion is expensive (more than 1500 dollars / L) and the thermoelectric performance of other conductive

polymers or composites is far from satisfactory (PF value < 50 μW/ (mK^2)) [16-18].

Graphene has a theoretical ZT value of about 4 at room temperature [19], which along with its excellent flexibility makes it an possible candidate for flexible thermoelectric applications. Since large-scale production of pure graphene sheets remains challenging, reduced graphene oxide (RGO) is employed as a substitute for graphene. As reported in previous work [20-22], the electrical conductivity of RGO sheets can be as high as 10^5 S/m, and the conductive type, bandgap and work function of RGO sheets can be adjusted by regulating the reduction degree of RGO sheets. Thus, RGO can be used as an effective component in thermoelectric nanocomposite, provided that graphene oxide (GO) sheets are reduced under proper condition.

RGO has been utilized in various kinds of thermoelectric materials as a beneficial composite additive [23-24], and the resulted RGO / inorganic nanocomposites indeed possess hopeful thermoelectric properties. However, the flexible thermoelectric films based on RGO / inorganic nanocomposites were barely reported. By coating RGO sheets with some surfactants, the dispersibility of RGO sheets in water can be greatly enhanced [25]. Consequently, it is possible to prepare the flexible thermoelectric film consisting of water-processable RGO and inorganic semiconductor. As a water-processable inorganic semiconductor with high Seebeck coefficient, tellurium nanowires (Te NWs) can be easily synthesized. Flexible films based on Te nanorods / polymer nanocomposite [26] and Te NWs / CNT nanocomposite [27] have also been reported in previous articles. However, the PF values of these films are also less than 30 μW/(mK^2) because of the low electrical conductivity or Seebeck coefficient. In this study, we demonstrate that high TE performance can be realized in the water-processable RGO/Te NWs hybrid films. The RGO sheets and Te NWs were prepared through hydrothermal reaction, respectively, then the RGO dispersion and Te dispersion were in sequence drop-cast on a piece of glass fiber sheet with aid of vacuum filtration to fabricate the hybrid thermoelectric film. The optimized hybrid film possessed the advantages of both components and achieved a much higher PF of 80 μW/(mK^2) than the previous hybrid films. Based on the measurement of Hall effect, the transport characteristics of hybrid films are analyzed and the excellent

thermoelectric performance possibly arises from the energy filtering effect in hybrid films.

2. Experimental

2.1. Materials

Graphene oxide (GO) was prepared by the modified Hummers' method [28]. The poly(sodium-p-styrenesulfonate) (NaPSS, M.W. 500k, analytical grade), sodium tellurite (Na_2TeO_3, 98%), aqueous ammonia ($NH_3 \cdot H_2O$, 25%), hydrazine hydrate ($N_2H_4 \cdot H_2O$, 98%), hydrobromic acid (HBr) solution (48%), acetone (99%) and polyvinylpyrrolidone (PVP, M.W. 30k, analytical grade) were purchased from Aladdin Chemical Co., Ltd. The glass fiber membranes were obtained from Yuyan (Shanghai) Chemical Co. All of these agents were used without further purification.

2.2. Preparation of RGO dispersion

25 mg of GO and 12.5 mg of NaPSS were dispersed in 12.5 mL of deionized water and the dispersion was ultra-sonicated for 10 min to form a homogeneous solution. Then 25 mL HBr solution was added into the brown dispersion and the mixture was heated in a sealed autoclave with a stainless steel shell at 120 ^{o}C for 4 h. The autoclave was naturally cooled to room temperature and resulted RGO sheets were obtained by vacuum filtration. After being washed by deionized water for several times, the black RGO sheets were dried in a vacuum oven at 60 ^{o}C for 5 h. Finally, the RGO sheets were dispersed in deionized water under ultra-sonication to form a black dispersion (2 mg/mL).

2.3. Preparation of Te nanowires dispersion

A typical procedure for preparation of Te NWs has been reported in our previous work [25], generally, 35 mL of deionized water was added into a 50 mL Teflon-lined stainless steel autoclave, then 1.0 g of PVP and 0.18 g of Na_2TeO_3 were dissolved in the water under vigorous magnetic stirring at room temperature. Subsequently, 1.7 mL of $N_2H_4 \cdot H_2O$ and 3.3 mL of $NH_3 \cdot H_2O$ were dropped into the solution. The obtained mixture was stirred for several minutes then the autoclave was sealed and maintained at 180 ^{o}C for 2 h. After the autoclave was cooled to room temperature by

flowing water, 75 mL of acetone was added into the solution to precipitate the Te NWs. The product was obtained after being centrifuged. The resulted Te NWs were dispersed in 20 mL deionized water to form a dark blue homogeneous dispersion (2 mg / mL).

2.4. Sample preparation

2.4.1 Fabrication of RGO films

The RGO sheets obtained from the 2 h hydrothermal reaction was named as RGO-2h, similarly, the RGO sheets obtained from the 4 h and 6 h hydrothermal reactions were named as RGO-4h and RGO-6h. First, the glass fiber membranes were cut to be small sheets (2.5 cm × 0.5 cm). Then, 5 drops (0.25 mL) of RGO-2h dispersion were drop-cast on the surface of glass fiber sheet with the aid of vacuum filtration. Finally, this RGO-2h film was dried in vacuum at 60 ^{o}C for 5 h. The RGO-4h film and RGO-6h film were obtained in the same way.

2.4.2 Fabrication of hybrid films

The glass fiber membrane was used as the substrate and a layered structure was applied in this experiment. First, the glass fiber membranes were cut to be small sheets (2.5 cm × 0.5 cm). Second, 5 drops (0.25 mL) of RGO-4h dispersion were drop-cast on the surface of glass fiber sheet with the aid of vacuum filtration. Then 2, 3, 4, 5,6 drops of Te dispersion were drop-cast on the glass fiber sheets coated with RGO. According to the amount of Te NWs in the sample, the hybrid film containing 2 drops of Te NWs was named as Te-2 in this work, and the Te wt% of this film is 28.5%. Similarly, other samples were named as Te-3 (Te wt% = 37.5%), Te-4 (Te wt% = 44.4%), Te-5 (Te wt% = 50%), and Te-6 (Te wt% =54.5%), respectively. The layered thermoelectric hybrid films have the following merits: (1) the thermal conductivity of glass fiber membrane is extremely low, which results in a relatively low thermal conductivity in the hybrid films; (2) the intimate contacts between the RGO sheets and the Te NWs are formed due to the well-distributed Te NWs on the smooth surface of RGO sheets.

2.5. Characterization

Transmission electron microscopy (TEM) images were obtained with a JEM

2100F transmission electron microscope under the operating voltage of 200 kV. The X-ray diffraction (XRD) patterns were collected using a film diffractometer equipped with a heating stage (PANalytical X'pert Pro MPD) and operated at 40 kV and 40 mA, with Cu Ka radiation (λ= 0.154 nm). Scanning electron microscopy (SEM) images were obtained with a Hitachi S-4800 FESEM microscope with an Oxford energy dispersive X-ray detector under the operating voltage of 2 kV. Raman spectra in the range of 750–2000 cm^{-1} were collected using a labRAM HR 800 and a 532 nm laser excitation wavelength. Electrical conductivities and Seebeck coefficients were measured by the static direct current (DC) method (ULVAC-RIKO, ZEM-3) under low argon (99.999%) atmosphere with temperature gradients of 20, 30 and 40 ^{o}C. Hall effect was measured with a Lakeshore 8404 Hall effect system.

3. Results and discussion

The electrical conductivities and Seebeck coefficients of RGO sheets obtained from 2 h, 4 h and 6 h hydrothermal reactions are displayed in Table 1. The Seebeck coefficient decreases while the electrical conductivity increases the reaction time. The RGO-6h film possesses the highest electrical conductivity of 10029 S/m. However, the dispersibility of RGO sheets in water reduced as the reaction time increases, which probably due to the decomposition of NaPSS during the hydrothermal reaction. Meanwhile, the PF value of RGO-4h film is the largest one, so the RGO-4h sheets were chosen to prepare the hybrid films.

Time of hydrothermal reaction (h)	Electrical conducivity (S/m)	Seebeck coefficient(μV/K)	PF value (μW/mK^2)
2	2145	15.2	0.50
4	6172	12.3	0.93
6	10029	8.7	0.76

Table 1. The electrical conductivities and Seebeck coefficients of RGO sheets obtained from 2 h, 4 h and 6 h hydrothermal reactions.

Figure 1 shows the detailed procedures of fabricating flexible hybrid films. Fig. 1A illustrates the preparation of dispersions of RGO and Te NWs, and the concentrations of these two dispersions are 2 mg / mL. The fabrication process of thermoelectric films based on RGO / Te NWs composites is shown in Fig. 1B. Briefly,

at first, the RGO dispersion was directly drop-cast on a piece of glass fiber sheet with the aid of vacuum filtration, then the Te NWs dispersion was drop-cast on the glass fiber sheet coated with RGO. After the water was dried in vacuum at 60 ^{o}C, the flexible hybrid films were obtained. The left optical image in Fig. 1C shows the high flexibility of hybrid film, and the right one is optical image of a 2 cm × 2cm hybrid film. This simple and water-processable vacuum filtration route is easily scaled up for wide applications.

The phase and morphology characterization of Te NWs are shown in Figure 2. Fig. 2A, B and C present the low-magnified and high resolution TEM (HRTEM) images of Te NWs, respectively. We can see the average diameter of Te NWs is around 12 nm. The HRTEM image of Te NWs is presented in Fig. 2C, and the lattice spacings of ca. 3.1 and 1.9 Å correspond to the lattice spacings of the (101) and (003) planes for Te, respectively. Also, the angle between the planes of (003) and (101) is 56.9°, which is consistent with the crystal structure. The XRD pattern of Te NWs is shown in Fig. 2D. All of the peaks can be exactly indexed to the hexagonal phase of Te with cell constants of a = 4.4579 Å, c = 5.927 Å, which are consistent with the standard literature data (JCPDF card number: 010-36-1452).

To explore the formation of hybrid films, the representative SEM images of a glass fiber sheet, RGO films and sample Te-5 are exhibited in Figure 3. As shown in Fig. 3A, the glass fiber sheet is made of interlaced glass fibers with different diameter. Fig. 3B, C and D show the formation of RGO film. Fig. 3B presents the surface of substrate coated with 1 drop of RGO dispersion. Some RGO sheets are attached on the glass fibers, but the substrate is barely covered by RGO sheets and the spaces among glass fibers are still obvious. The surface of substrate coated with 3 drops of RGO dispersion is shown in Fig. 3C. The surface of substrate has been covered by RGO sheets and only the profiles of several glass fibers can be observed. As shown in Fig. 3D, With the amount of RGO dispersion increasing to 5 drops, the surface of substrate has been completely covered by the relatively smooth RGO sheets and the glass fibers are scarcely observed. Fig. 3E illustrates the surface of sample Te-5. All the Te NWs are packing densely on surface of RGO film and the hybrid film

possesses a relative smooth surface. The average length of Te NWs is about 10 μm and they are tightly connected with each other to form a network. Fig. 3F shows the cross-section of sample Te-5.The RGO layer is too thin to be observed, while it is clear that Te NWs are mounted layer upon layer and the thickness of film is about 800 nm.

The XRD patterns of RGO and hybrid films with different amounts of Te NWs are shown in Figure 4. The RGO film displays a strong, broad peak at 2θ = 26.2° and a weak, broad peak at 2θ = 42.1°, respectively. These two peaks correspond to the (002) and (101) plane of graphite and the broadening of these two peaks is due to the amorphous structures in RGO sheets [29]. All the XRD spectra of hybrid films are similar to that of pure Te NWs, and the bump between 2θ = 15° and 2θ = 35° arises from the diffraction from RGO sheets in hybrid films.

Figure 5 illustrates the Raman spectra of RGO film and hybrid films. On the excitation by 532 nm laser, all of the spectra display two prominent peaks at 1351cm^{-1} (D band) and 1596 cm^{-1} (G band). Moreover, a shoulder peak, named as D' band, locates beside G band at 1607 cm^{-1}. On the other hand, the intensity ratios of D band to G band (I_D/I_G) increase with the increased amount of Te NWs in hybrid films, which are shown in Table 2. The G band is due to the first order scattering from the doubly degenerate E_{2g} phonon modes of graphite at the Brillouin zone center and is characteristic of all sp^2-hybridized carbon networks, and the dispersive D band arises from phonon branches within the interior of the graphite Brillouin zone that are activated by scattering from defects [30], thus the I_D/I_G ratio can work as a sensitive measure of the disorder and crystallite size of the graphitic layers. The I_D/I_G values increase from 1.28 (RGO) to 1.41 (Te-6), indicating that more defects are created in RGO films with the increased amount of Te NWs in hybrid films. Meanwhile, the D' band gradually becomes obvious in Raman spectra of hybrid films, which implies that highly defective structures have been formed in the RGO sheets [31].

Sample	I_D/I_G
RGO	1.28
Te-2	1.35
Te-3	1.37
Te-4	1.38
Te-5	1.40
Te-6	1.41

Table 2. The I_D/I_G values of RGO and hybrid films with different amount of Te NWs.

The electrical conductivities, Seebeck coefficients and PF values of RGO films and hybrid films were measured at 40 ^oC. As reported in our previous work [25], the electrical conductivity and Seebeck coefficient of pure Te NWs film were 8 S/m and 402 μV/ K, respectively. The thermoelectric properties of RGO film and Te NWs film are displayed in Table 3. Shown in Figure 6 is the electrical conductivity and Seebeck coefficient as a function of weight percentage of Te NWs drop-cast in hybrid films and the error range is ± 7%. With increasing the amount of Te NWs in hybrid films, the electrical conductivity decreases and Seebeck coefficient increases. The hybrid film with 28.5 wt% of Te NWs dispersion (Te-2) possesses the highest electrical conductivity of 1381 S/m, which is much higher than that of pure Te NWs. On the other hand, the Seebeck coefficient of hybrid film with 54.5 wt% of Te NWs dispersion (Te-6) is about 40 times higher than that of RGO films, which reaches as high as 298 μV/K.

The PF values of hybrid films are shown in Figure 7 and the error range is also ± 7%. With increasing the amount of Te NWs in the hybrid films, the PF value initially increases to a maximum, then it turns to decrease with the amount of Te NWs. Since the high electrical conductivity of RGO sheets and the high Seebeck coefficient of Te NWs have been integrated in hybrid films, all the PF values of hybrid films are larger than that of pure RGO film or Te NWs film, and the hybrid film with 50 wt% of Te NWs dispersion (Te-5) possesses the highest PF value of 80 $\mu W/(mK^2)$. The thermoelectric performance of sample Te-5 is compared with that of RGO film and

Te NWs films in Table 3.

	Electrical conductivity (S/m)	Seebeck coefficient (μV/K)	PF values (μW/mK^2)
Te NWs film	8	402	1.29
RGO film	6172	12	0.93
Te-5	978	286	80

Table 3. The thermoelectric properties of Te NWs film, RGO film and sample Te-5.

To test the flexibility of hybrid films, the resistance R_b as a function of bending radius (R) for random hybrid films is shown in Figure 8, where R_0 is the corresponding value of its original state before bending and the error range is ±1%. As shown in this figure, after being bent, the average resistance of hybrid films increases slightly, indicating that the hybrid films possess flexibility and reliability.

The distinct enhancement of PF value in hybrid films is worth investigating. The optimized electrical conductivity of hybrid film is more than one hundred times higher than that of Te NWs film, while its Seebeck coefficient is about as high as three-quarters of Seebeck coefficient of Te NWs. Thus, the improvement of TE properties in hybrid films are not merely associated with the physical mixing of Te NWs and RGO sheets. To explain the transport characteristics of charge carrier in hybrid films, the Hall effects of RGO film and hybrid films were measured. As shown in Figure 9, the RGO film possesses the highest carrier concentration and the smallest carrier mobility. With the increased amount of Te NWs in hybrid films, the carrier concentration decreases while the carrier mobility increases. It is well known that the σ is calculated as $\sigma = \eta e \mu_{(\varepsilon)}$, where η is carrier concentration, e is the charge and $\mu(\varepsilon)$ is the carrier mobility. Since the carrier concentration of RGO film is several orders of magnitude higher than that of hybrid films, it is certain that RGO film possesses much higher electrical conductivity than hybrid films. Meanwhile, the decreasing rate of the carrier concentration is lower than the increasing rate of the carrier mobility, so the electrical conductivity decreases when the content of Te NWs dispersion increases from 0 to 54.5 wt%. Seebeck coefficient is inversely proportional to the carrier

concentration and with the deceased carrier concentration, an improvement of carrier mobility generally leads to an enhanced Seebeck coefficient. Thus, it is easy to understand that the Seebeck coefficient increases with the increased amount of Te NWs in hybrid films.

As exhibited in Figure 10, the possible carrier transport in RGO / Te NWs hybrid system is graphically represented. The positive sign of the Seebeck coefficients in both of RGO sheets and Te NWs is related to the p-type character of the semiconductor, so the carrier in hybrid films is hole. Since the RGO sheets possess high carrier concentration while the Te NWs possess high carrier mobility, the Te NWs network acts as the highway for holes to quickly transport from one piece of RGO sheet to another one. The high-energy holes can transfer cross the energy barrier while the low-energy holes are scattered by the energy barrier. The carrier concentrations of hybrid films are lower than RGO film but higher than Te NWs film. As a consequence, both of their respective virtues can be combined in hybrid films and the PF values of hybrid films are better than either component.

Conclusions

Using the glass fiber sheets as substrates, the water-processable RGO/Te NWs hybrid films with superior TE properties are prepared in this work. The hybrid films show better TE performance than either one of RGO film and Te film, and the optimized PF value reaches 80 $\mu W/(mK^2)$ at 40^oC. The transport characteristics of charge carrier in this hybrid system is investigated based on the measurement of Hall effect. This article provides a possible access to high-performance and flexible TE films based on RGO and inorganic semiconductors. It is believed that the thermoelectric performance of this RGO/ inorganic NWs based thermoelectric hybrid film can be further improved by using other inorganic NWs that having better thermoelectric performance.

Acknowledgements

This work was supported by National Natural Science Foundation of China (Grant No. 51572049, 51562005) and Guangxi Natural Science Foundation of China

(Grant No. 2015GXNSFFA139002).

References

1. L. E. Bell, *Science*, 2008, 321, 1457.

2. I. Levesque and P. O. Bertrand, *Chem. Mater.*, 2007, 19, 2128.

3.Y. Z. Pei, A. D. LaLonde, N. A. Heinz, X. Y. Shi, S. Iwanaga, H. Wang, L. D. Chen and G. J. Snyder, *Adv. Mater.*, 2011, 23, 5674.

4. P. J. Taroni, I. Hoces, N. Stingelin, M. Heeney, and E. Bilotti, *Isr. J. Chem.*, 2013, 53, 1.

5. S. L. Kim, K. Choi, A. Tazebay, and C. Yu, *ACS Nano*, 2014, 8, 2377.

6. C. Dun, C. Hewitt, H. Huang, J. Xu, D. Montgomery, W. Nie, Q. Jiang, and D. L. Carroll, *ACS Appl. Mater. Interfaces*, 2015, 7, 7054.

7. K. Kato , Y. Hatasako , M. Uchino, Y. Nakata , Y. Suzuki , T. Hayakawa , C. Adachi , and K. Miyazaki, *Adv. Mater. Interfaces*, 2014, 1, 1300015.

8. W. Zhao, H. T. Tan, L. P. Tan, S. Fan, H. H. Hng, Y. C. F. Boey, I. Beloborodov, and Q. Yan, *ACS Appl. Mater. Interfaces*, 2014, 6, 4940.

9. Y. Du, S.Z. Shen, K.F. Cai and P.S. Casey, *Prog. Polym. Sci.*, 2012, 37, 820.

10. B. T. McGrail, A. Sehirlioglu, and E. Pentzer, *Angew. Chem. Int. Ed.*, 2015, 54, 1710.

11. O. Bubnova, Z. U. Khan, A. Malti, S. Braun, M. Fahlman, M. Berggren and X. Crispin, *Nat. Mater.*, 2011, 10, 429.

12. G. H. Kim, L. Shao, K. Zhang, and K. P. Pipe, *Nat. Mater.* 2013, 12, 719.

13. Q. Yao, L. D. Chen, W. Q. Zhang, S. C. Liufu, and X. H. Chen, *ACS nano*, 2010, 4, 2445.

14. K.C. See, J.P. Feser, C.E. Chen, A. Majumdar, J.J. Urban, and R.A. Segalman, *Nano Lett.* 2010, 10, 4664.

15. M. He, J. Ge, Z.Q. Lin, X.H. Feng, X.W. Wang, H.B. Lu, Y. L. Yang and F. Qiu, *Energy Environ. Sci.*, 2012, 5, 8351.

16. Y. Du, K. F. Cai, S. Chen, P. Cizek, and T. Lin, *ACS Appl. Mater. Interfaces*, 2014, 6, 5735.

17. Y. Zhao, G. S. Tang, Z. Z.Yu and J. S. Qi, *Carbon*, 2012, 50, 3064.

18. K. Suemori, Y. Watanabe and S. Hoshino, *Appl. Phys. Lett.* 2015, 106, 113902.

19. W. Liu, Q. Jie, H. S. Kim and Z. Ren, *Acta Mater.*, 2015, 87, 357.

20. S. F. Pei, J. P. Zhao, J. H. Du, W. C. Ren, and H. M. Cheng, *Carbon*, 2010, 48, 4466–4474.

21. J. Gao, C. Y. Liu, L. Miao, X. Y. Wang, and Y. Chen, *J. Electron. Mater.*, 2015, DOI: 10.1007/s11664-015-4000-5.

22. P. V. Kumar, M. Bernardi, and J. C. Grossman, ACS Nano, 2013, 7, 1638–1645.

23. H. Ju and J. Kim, *Dalton Trans.*, 2015, 44, 11755.

24. A. Dey, S. Panja, A. K. Sikder and S. Chattopadhyay, *RSC Adv.*, 2015, 5, 10358.

25. J, Gao, C. Y. Liu, L. Miao, X. Y. Wang, C. Li, R. Huang, Y. Chen, and S. Tanemura, *Synthetic Met.*, 2015, 210, 342.

26. C. J. Zhou, C. C. Dun, Q. Wang, K. Wang, Z. Q. Shi, D. L. Carroll, G. W. Liu, and G. J. Qiao, *ACS Appl. Mater.* Interfaces, 2015, 7, 21015.

27. J. Choi, J. Y. Lee, H, Lee, C. R. Park and H. Kim, *Synthetic Met.*, 2014, 198, 340.

28. D. C. Marcano, D.V. Kosynkin, J. M. Berlin, A. Sinitskii, Z. Z. Sun, A. Slesarev, L. B. Alemany, W. Lu and J. M. Tourl, ACS Nano, 2010, 4, 4806.

29. J. F. Liu, D. Takeshia, K. Sasakia, and S. M. Lyth, *J. Electrochem. Soc.* 2014, 161, 838.

30. A.C. Ferrari, J.C. Meyer, V. Scardaci, C. Casiraghi, M. Lazzeri and F. Mauri, *Phys. Rev. Lett.* 2006, 97, 187401.

31. A. Kaniyoor and S. Ramaprabhu, *AIP Advances*, 2012, 2, 032183.

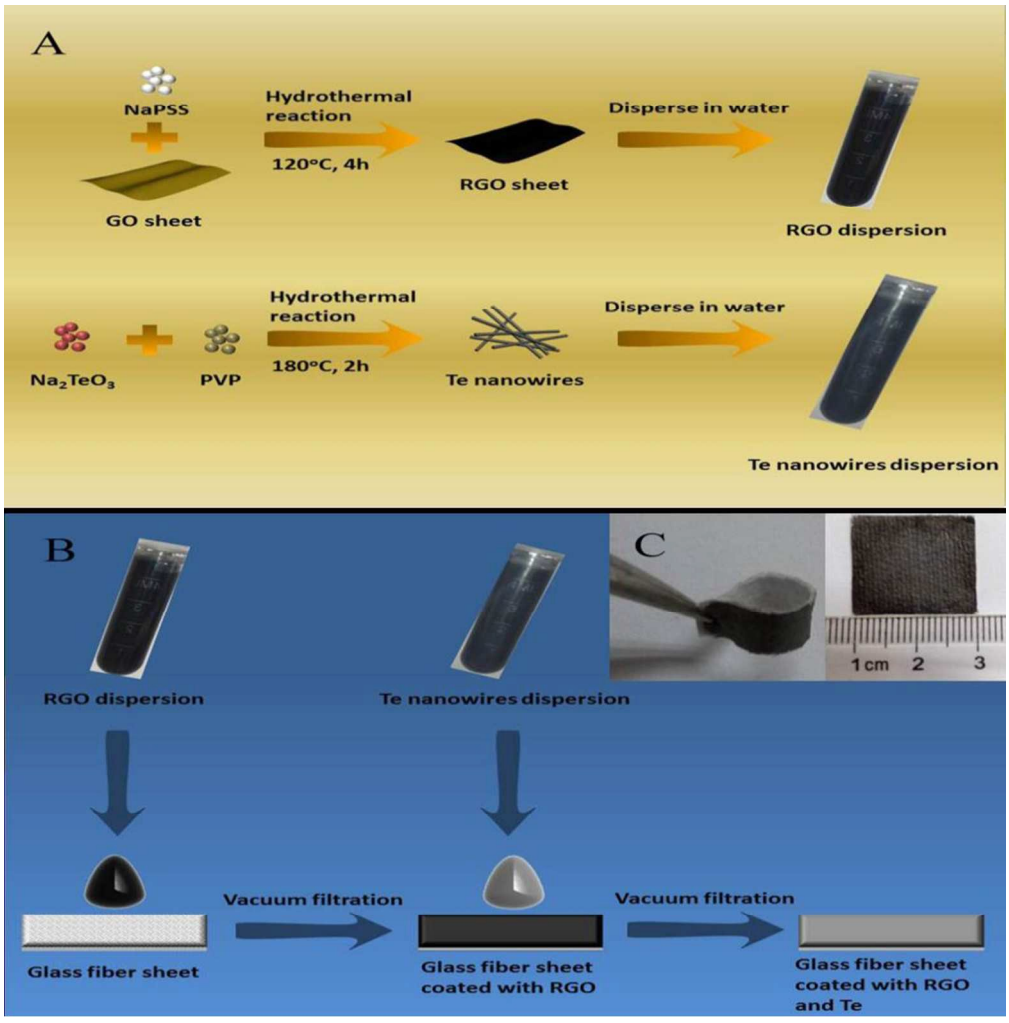

Figure 1. (A) The preparation of RGO dispersion and Te nanowires (Te NWs) dispersion. (B) The fabrication of RGO/Te hybrid films on glass fiber sheets. (C) Optical images of bent RGO/Te hybrid film (left, 0.5 cm × 2cm) and a 2 cm × 2cm hybrid film (right).
127x128mm (220 x 220 DPI)

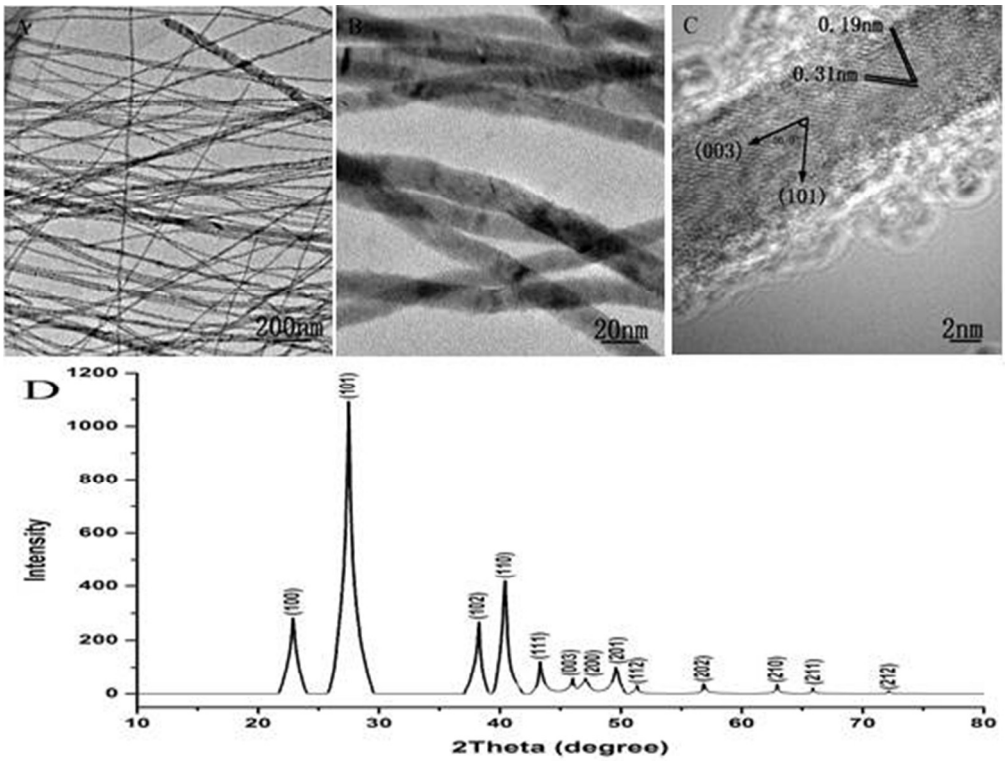

Figure 2. TEM images of TeNWs (A and B), and HRTEM image of Te NWs (C), and XRD spectrum of Te NWs (D).
146x111mm (96 x 96 DPI)

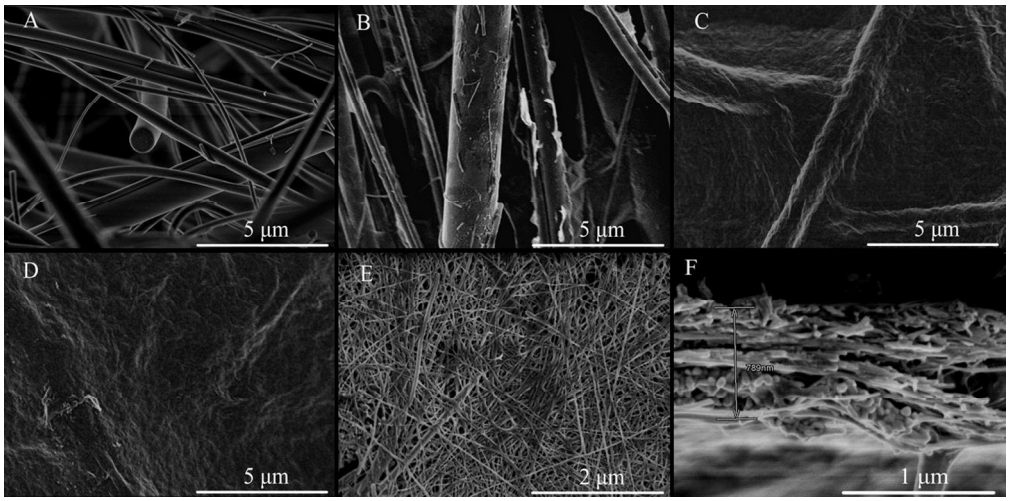

Figure 3. Representative SEM images of glass fiber sheet (A), glass fiber sheets coated with 1, 3 and 5 drops of RGO dispersions (B, C, and D), and sample Te-5 (E and F).
224x109mm (150 x 150 DPI)

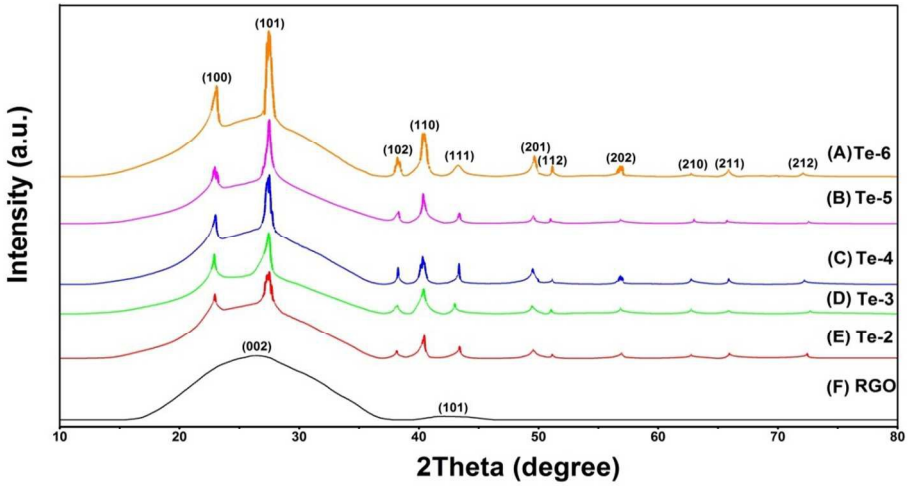

Figure 4. The XRD patterns of RGO and hybrid films with different amount of Te NWs (A) Te-6, (B) Te-5, (C) Te-4, (D) Te-3, (E) Te-2, (F) RGO.
145x83mm (220 x 220 DPI)

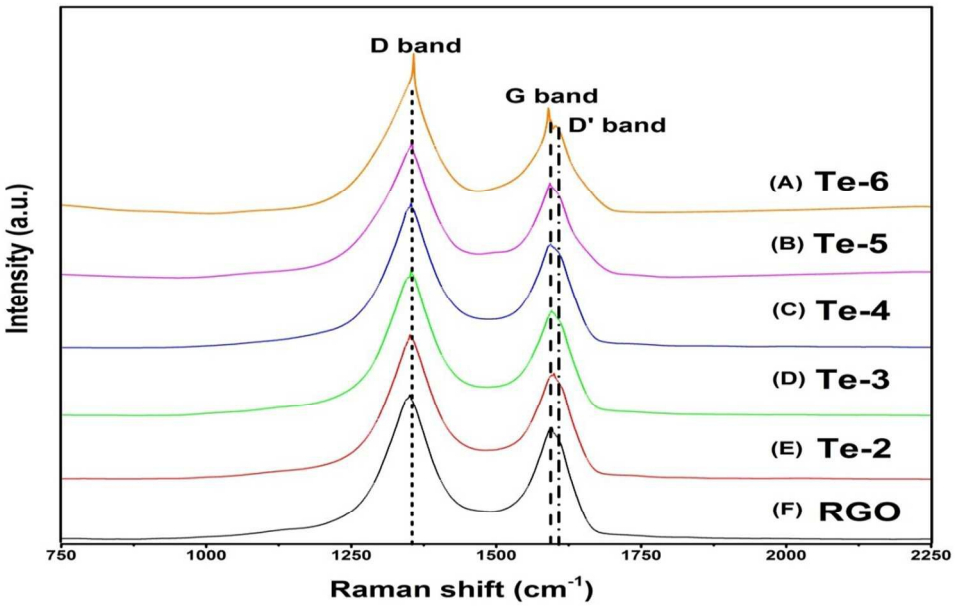

Figure 5. The Raman spectra of RGO and hybrid films with different amount of Te NWs (A) Te-6, (B) Te-5, (C) Te-4, (D) Te-3, (E) Te-2, (F) RGO.
142x91mm (220 x 220 DPI)

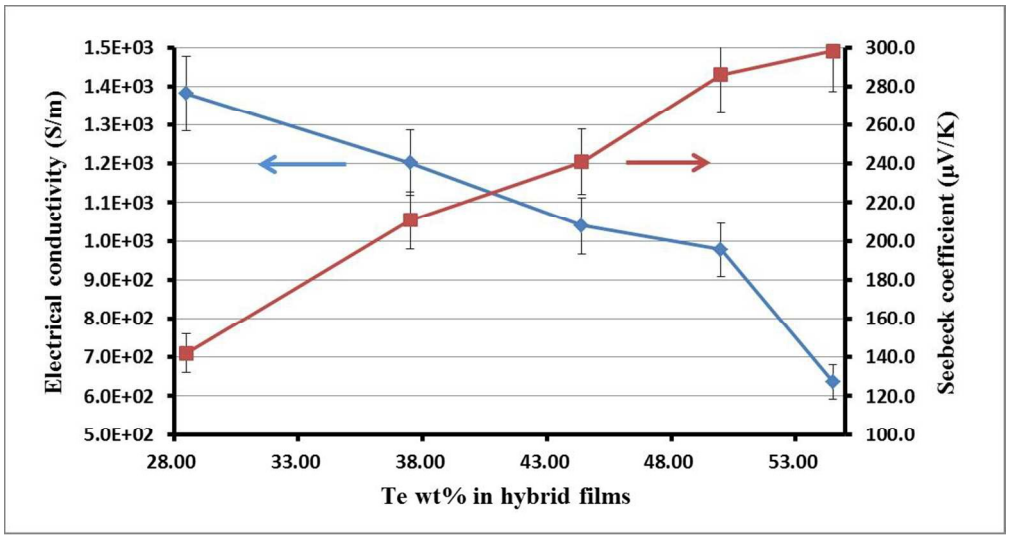

Figure 6. The electrical conductivities and Seebeck coefficients of hybrid films with different amounts of Te NWs.
197x104mm (150 x 150 DPI)

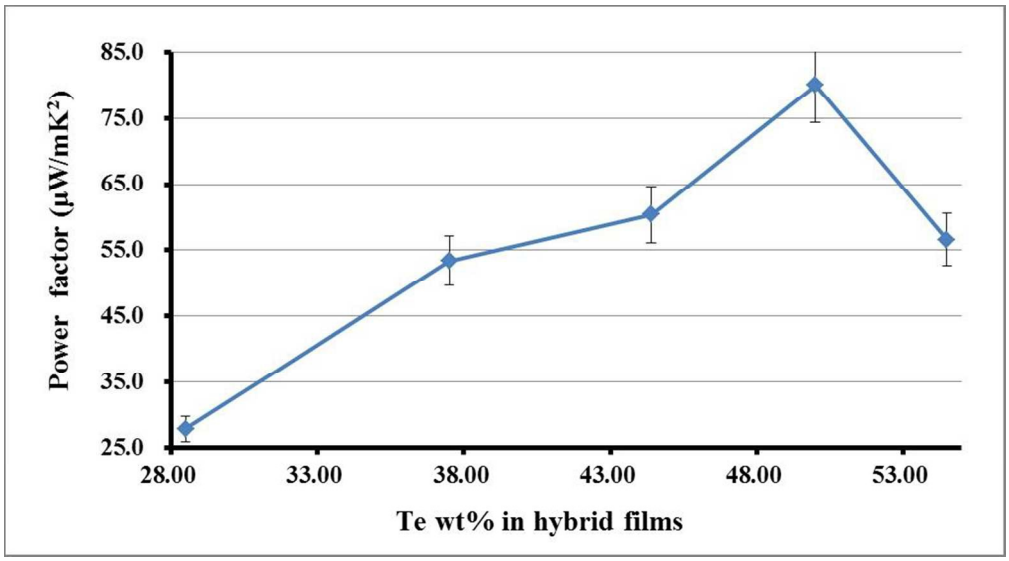

Figure 7. The PF values of hybrid films with different amounts of Te NWs.
171x94mm (150 x 150 DPI)

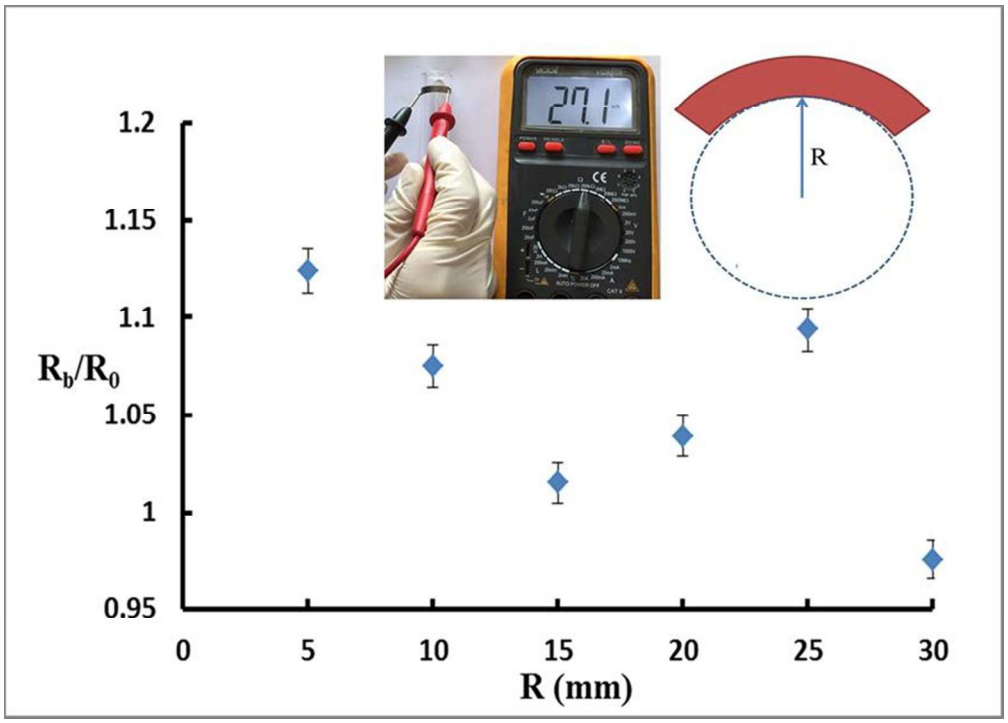

Figure 8. The resistance R_b as a function of bending radius (R) for random hybrid films, where R_0 is the corresponding value of its original state before bending.
146x104mm (150 x 150 DPI)

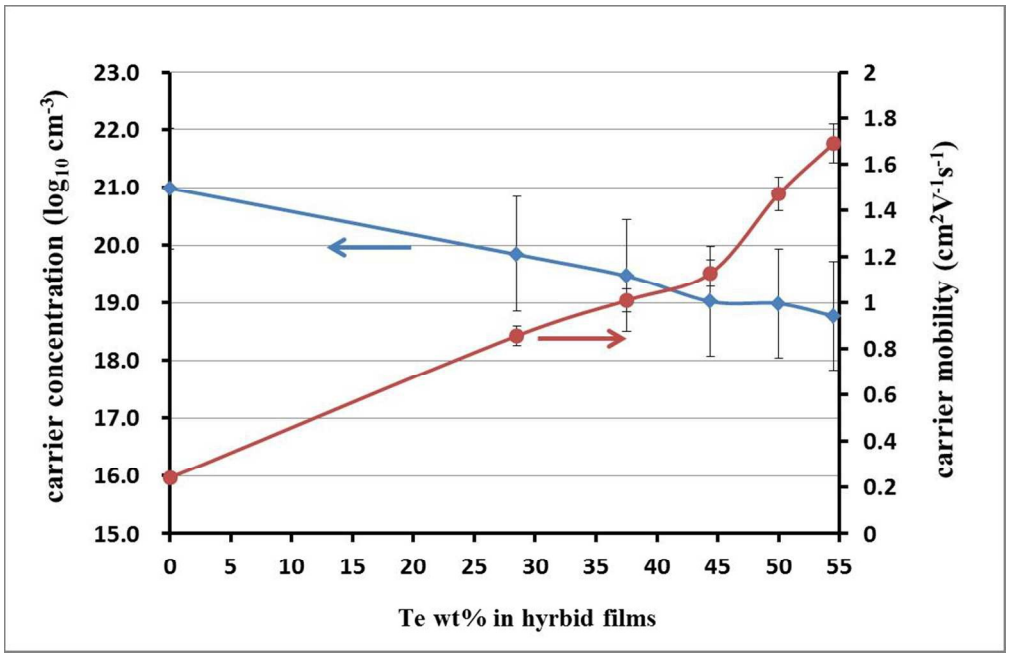

Figure 9. The carrier concentration and mobility of RGO film and hybrid films with different amounts of Te NWs.
191x123mm (150 x 150 DPI)

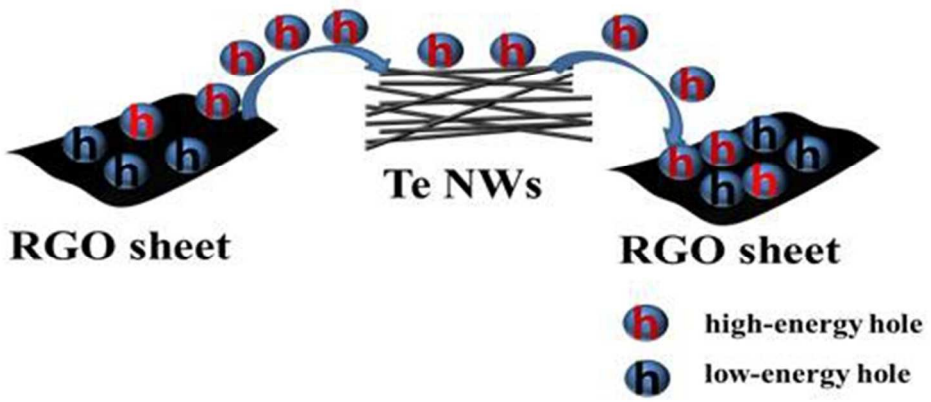

Figure 10. The graphical representation of carrier transport in RGO / Te NWs hybrid system.
142x64mm (96 x 96 DPI)

Table of contents

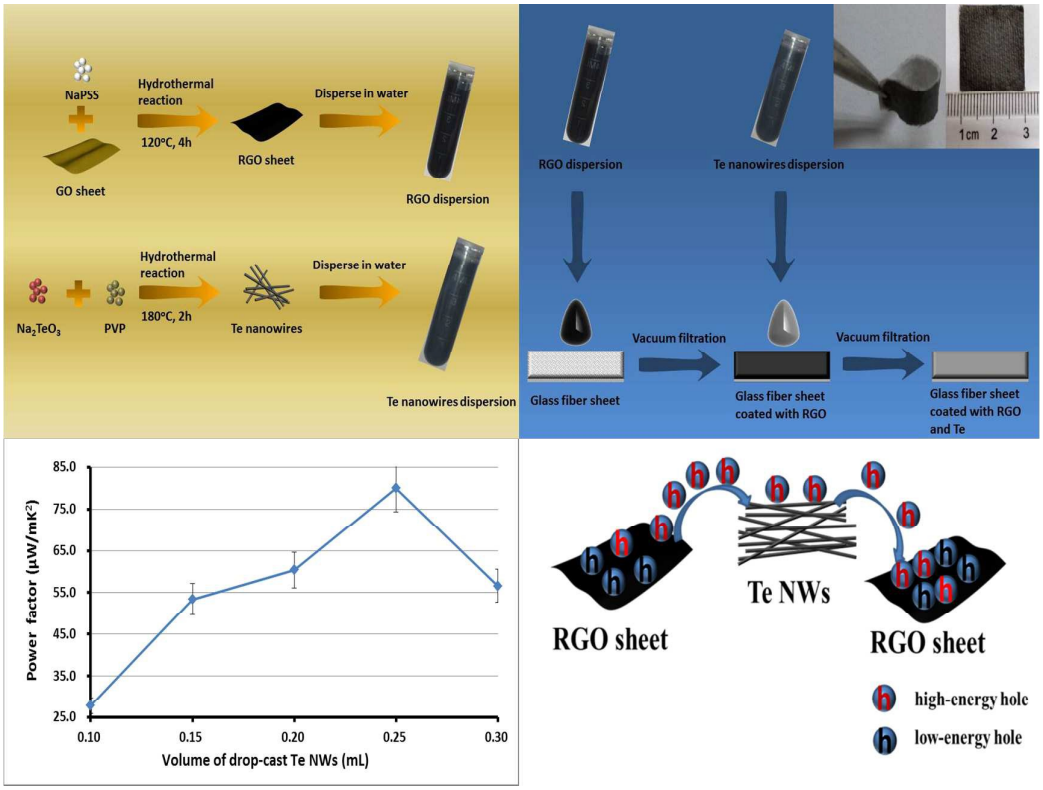

Text:

Highly-flexible RGO/Te NWs hybrid films with superior thermoelectric performance (optimal PF value = 80 μW/(mK^2)) were fabricated and the transport characteristics of charge carrier was investigated.